



Bacterial outer membrane vesicles-based therapeutic platform eradicates triple-negative breast tumor by combinational photodynamic/chemo-/immunotherapy

Yongjiang Li^{a,b,1}, Junyong Wu^{a,b,1}, Xiaohan Qiu^{a,b}, Suhe Dong^c, Jun He^d, Jihua Liu^{a,b}, Wenjie Xu^{a,b}, Si Huang^{a,b}, Xiongbin Hu^{a,b}, Da-Xiong Xiang^{a,b,*}

^a Department of Pharmacy, the Second Xiangya Hospital of Central South University, Changsha, China

^b Hunan Provincial Engineering Research Centre of Translational Medicine and Innovative Drug, Changsha, China

^c The PLA Rocket Force Characteristic Medical Center, Beijing, China

^d Department of Liver Surgery, the Second Xiangya Hospital of Central South University, Changsha, China

ARTICLE INFO

Keywords:

Bacterial outer membrane vesicles
Bioengineering
Drug delivery
Macrophage
Pyroptosis
Tumor microenvironment

ABSTRACT

Bacterial outer membrane vesicles (OMVs) are potent immuno-stimulating agents and have the potentials to be bioengineered as platforms for antitumor nanomedicine. In this study, OMVs are demonstrated as promising antitumor therapeutics. OMVs can lead to beneficial M2-to-M1 polarization of macrophages and induce pyroptosis to enhance antitumor immunity, but the therapeutic window of OMVs is narrow for its toxicity. We propose a bioengineering strategy to enhance the tumor-targeting ability of OMVs by macrophage-mediated delivery and improve the antitumor efficacy by co-loading of photosensitizer chlorin e6 (Ce6) and chemotherapeutic drug doxorubicin (DOX) into OMVs as a therapeutic platform. We demonstrate that systemic injection of the DOX/Ce6-OMVs@M therapeutic platform, providing combinational photodynamic/chemo-/immunotherapy, eradicates triple-negative breast tumors in mice without side effects. Importantly, this strategy also effectively prevents tumor metastasis to the lung. This OMVs-based strategy with bioengineering may serve as a powerful therapeutic platform for a synergic antitumor therapy.

1. Introduction

Cancer is a leading cause of human death with increasing mortality. Breast cancer is the most commonly diagnosed cancer in women worldwide [1]. Triple-negative breast cancer (TNBC), a subtype of breast cancer, is highly invasive with high metastasis risks and poor prognosis [2]. The development of new therapeutic strategies for TNBC is urgent in the clinic. Immunotherapy has emerged as a promising strategy for cancer management by harnessing the immune system [3], blocking suppressive immune-checkpoint pathways [4], or triggering antigen-specific immune responses in tumors [5]. However, the reported antitumor efficiency of current immunotherapy in patients with TNBC has not been satisfactory [6]. In clinical settings, immunotherapy can be applied as a complementary strategy and is usually combined with other conventional radiotherapy and/or chemotherapy for TNBC [7].

Therefore, the development of novel and potent antitumor therapy combining multiple strategies is of great significance for TNBC management.

In the 1890's, William Coley firstly used the components from attenuated bacteria for tumor therapy [8]. The successful activation of the immune system via bacterial components stimulation suppressed the tumor growth in patients. Although promising, the infection risks of bacteria and the toxicity limited the application and development of bacteria-based antitumor immunotherapy. In recent years, with the understanding of extracellular vesicles (EVs), bacteria-derived outer membrane vesicles (OMVs) are emerging as alternatives to bacteria with decreased infection risk while maintaining the immuno-stimulating activity [9].

OMVs are natural spherical vesicles secreted by Gram-negative bacteria, with a diameter of 30–250 nm. OMVs are originated from

Peer review under responsibility of KeAi Communications Co., Ltd.

* Corresponding author. Department of Pharmacy, the Second Xiangya Hospital of Central South University, 139 Middle Renmin Road, Changsha, 410011, China.

E-mail address: xiangdaxiong@csu.edu.cn (D.-X. Xiang).

¹ Contribute equally to this work.

<https://doi.org/10.1016/j.bioactmat.2022.05.037>

Received 30 November 2021; Received in revised form 14 May 2022; Accepted 28 May 2022

2452-199X/© 2022 The Authors. Publishing services by Elsevier B.V. on behalf of KeAi Communications Co. Ltd. This is an open access article under the CC BY-NC-ND license (<http://creativecommons.org/licenses/by-nc-nd/4.0/>).

the outer membrane and contain a variety of biomolecules from the periplasm and membrane of the parental bacteria [10]. OMVs play important roles in the bacterial defense system and maintenance of bacterial communities. Besides, OMVs, possessing multiple bacteria biomolecules, are highly immunogenic and have high lymph node entry and (antigen-presenting cell) APC uptake efficiency, making them attractive platforms for antigen delivery and vaccination [11,12]. OMVs-based vaccines such as MeNZB and Bexsero have shown excellent efficacy against infections with high safety [13]. OMVs can also induce systemic immune responses and recruit nonspecifically activated immune cells to initiate the antitumor response, suggesting that OMVs can be explored as tumor immunotherapeutic platforms [14].

Escherichia coli (*E. coli*) is one of the most important bacteria tools in biotechnology, bioengineering, and the pharmaceutical industry [15]. OMVs derived from *E. coli* are emerging in the field of nanomedicine for their natural components and nano-size [16]. OMVs have been explored as nanocarriers for efficient cargo delivery [17]. However, tumors possess complex immune microenvironments and a strong capacity for immune evasion [18], and safety is still a major concern for the use of OMVs for therapeutic purposes because of their toxin components, such as LPS, from parental bacteria [19].

In this study, OMVs showed potent antitumor potentials in preliminary evaluations, but the therapeutic window is narrow and safety remains a major limitation for its application. We enhanced the tumor-targeting ability of OMVs by macrophages-mediated delivery and improved the antitumor efficacy by co-loading of photosensitizer chlorin e6 (Ce6) and doxorubicin (DOX) into OMVs for combinational photodynamic/chemo-/immunotherapy. The potential antitumor mechanisms of OMVs were demonstrated to be associated with shifting macrophage M2-to-M1 polarization and inducing pyroptosis in the tumor. Findings from this study supported that OMVs are promising platforms for the management of TNBC.

2. Materials and methods

2.1. Bacteria strains, cell culture and animals

E. coli (DH5 α) was purchased from Fenghui Bio (Changsha, China) and cultured on Columbia Blood Agar Base (BioIVD, Zhengzhou, China). 4T1 murine mammary carcinoma cells were maintained in RPMI 1640 medium containing GlutaMAXTM and Sodium Pyruvate 0.11 g/L (Invitrogen) and supplemented with 10% fetal bovine serum (FBS, Biological Industries, Sartorius). Murine Raw264.7 macrophages were maintained in Dulbecco's modified Eagle's minimum essential medium (DMEM) supplemented with 10% FBS. Cells were incubated at 37 °C in humidified air with 5% CO₂. Female BALB/C mice (6 weeks old) were obtained from SJA Laboratory Animal Co., LTD (Changsha, China) and housed following the guidelines of the Institutional Animal Care and Use Committee (IACUC). Animal studies were performed according to the protocols approved by the Institutional Animal Care and Use Committees of the Department of Laboratory Animals of the Second Xiangya Hospital of Central South University (No. 2021103).

2.2. OMV preparation and characterization

A single colony of *E. coli* (DH5 α) after grown on Columbia Blood Agar Base for 24 h was collected and inoculated into LB medium (Hangzhou Microbial Reagent Co., LTD, China) at 37 °C followed by culturing in a rotary shaker at 37 °C for 12 h then refreshed with LB medium at 1:100 dilution. Bacterial culture medium in shake flask was collected until the OD600 value reached 1. OMVs were prepared as previously described with modification [20]. Briefly, 4 L of collected bacterial culture medium was centrifuged at 10,000 g for 10 min to remove the bacteria, followed by filtering through a 0.22 μ m filter (Millipore, USA). The filtrate was then concentrated by using centrifugal filters with a molecular weight cutoff (MWCO) of 100 kDa (Millipore, USA). The

concentrated medium was then processed by ultracentrifugation at 200,000 g for 4 h at 4 °C (XPN, Beckman Coulter, USA). The OMVs pellet was resuspended using PBS. The protein concentration of OMVs was determined by using BCA Protein Assay Kit (Beyotime, China). OMVs samples were stored at –80 °C.

OMVs were characterized by size, TEM imaging and protein profiles. Size distribution and polydispersed index (PDI) of OMVs were analyzed using Zetasizer Nano (ZS90, Malvern, UK). Also, nanoparticle tracking analysis (NTA) was performed to assess the size distribution and particle concentration of OMVs (Nanosight NS300, Malvern, UK). We also used the Pierce Chromogenic Endotoxin Quant Kit (ThermoFisher, USA) to measure OMV samples at equivalent particle concentration to quantify the lipopolysaccharide (LPS). Morphology of OMVs was observed by transmission electron microscopy (TEM). Images were captured using a Tecnai G2 Spirit TWIN Electron Microscope (FEI, Holland). Protein profiles of OMVs were observed by Coomassie brilliant blue staining and analyzed using a gel imaging system (ChemiDocTM Touch, Bio-Rad, USA).

2.3. Preliminary evaluation of safety and antitumor potentials of OMVs

The Antitumor efficacy of free OMVs was evaluated in mice with orthotopic breast tumors. Animal models were developed as previously described [21]. Briefly, breast tumors were orthotopically implanted by injecting 1×10^7 4T1 cells into the fourth right mammary fat pad of female BALB/C mice (six-week-old). After tumor volume reached 200 mm³ (about 10 days), mice were treated once with different doses (OMVs-L: 0.25×10^{12} particles; OMVs-M: 0.50×10^{12} particles; OMVs-H: 1.00×10^{12} particles) of OMVs via *i.v.* injection. Tumor growth and mice bodyweight were recorded every day. Tumors and spleen were collected and weighted. Tumors were fixed in 4% PFA and sliced and stained with H&E. Blood samples were collected for enzyme linked immunosorbent assay (ELISA) of IL-6, TNF- α and IFN- γ (Boster Biological Technology, Wuhan, China) to assess the immune response. Besides, the relative levels of alanine aminotransferase (ALT) and aspartate aminotransferase (AST) reflect liver functions, and blood urea nitrogen (BUN) and creatinine (Cr) to reflect renal functions were analyzed. Liver and spleen tissues were also collected and fixed in 4% PFA and sliced and stained with H&E.

2.4. Preparation and characterization of OMVs@M

We firstly investigated the cytotoxicity of OMVs to macrophages by CCK-8 assay. RAW 264.7 cells were seeded into 96-well plates at a density of 5×10^3 cells per well and then incubated with OMVs for 24 h. Cell viability was assessed by the CCK8 Assay (NCM biotech, China) by measuring the absorbance at 450 nm using an Infinite F50 microplate reader (Tecan, Switzerland). After confirming the safety of OMVs loading and estimating the loading capacity, OMVs were loaded into macrophages by direct incubation. OMVs were added to the cell culture medium and taken up by macrophages. Following the different dose of OMVs, OMVs@M were prepared as: OMVs@M-L: 0.25×10^{12} OMV particles loaded in 1×10^6 macrophages; OMVs@M-M: 0.50×10^{12} OMV particles loaded in 2.5×10^6 macrophages; OMVs@M-H: 1.00×10^{12} OMV particles loaded in 3.5×10^6 macrophages. To observe OMVs in macrophages, OMVs@M were fixed by mixing with a solution containing 4% PFA and 2.5% glutaraldehyde and then observed by TEM. Further, fluorescence microscopy was performed to observe Pkh67-labeled OMVs loaded in macrophages. Protein profiles of OMVs@M were observed by Coomassie brilliant blue (Beyotime, China) staining.

2.5. Macrophage migration and in vivo biodistribution

To evaluate macrophage migration, a transwell migration assay was performed. 4T1 tumor cells were cultured in the lower chamber (2×10^5 cells per well) while Pkh67-labeled Raw264.7 macrophages were

cultured in the upper chamber (1×10^5 cells per well) after incubation with OMVs or PBS for 6 h. After 24 h for migration, cells in the lower chamber were washed with PBS three times and then fixed with 4% PFA for 15 min. PFA was removed and cells were washed with PBS three times, nuclei were stained by DAPI (5 $\mu\text{g/mL}$, Beyotime, China). Cells were subjected to fluorescence microscopy to observe macrophage migration. For *in vivo* biodistribution study, OMVs were labeled by DiR by incubation for 2 h, excessive unbound dyes were removed by ultrafiltration through centrifugal filters (100 kDa). DiR-labeled OMVs were incubated with macrophages to produce DiR-OMVs@M. Breast tumor-bearing mice were administrated with DiR-OMVs@M or DiR-OMVs or free DiR via *i.v.* injection. 8 h post-injection, fluorescence was measured using the IVIS Spectrum (PerkinElmer, USA). *Ex vivo* biodistribution of DiR-OMVs and DiR-OMVs@M in tumors and other major organs were also inspected.

2.6. Improved safety and antitumor efficacy of OMVs@M

Similar to the preliminary *in vivo* evaluation of OMVs, after 10 days of tumor cell implantation, tumor-bearing mice were treated once with different doses of OMVs@M via *i.v.* injection. Tumor growth and mice bodyweight were recorded every day. Tumors and spleen were collected and weighted. Tumors were fixed in 4% PFA and sliced and stained with H&E. Blood samples were collected for ELISA of IL-6, TNF- α and IFN- γ .

2.7. Development of Ce6/DOX-OMVs@M

To further improve the antitumor efficacy of OMVs@M, photosensitizer Ce6 and chemotherapeutic drug doxorubicin (DOX) were encapsulated into OMVs and then loaded into macrophages for laser-triggered release and combined photo/chemo/immunotherapy. Ce6 (400 $\mu\text{g/mL}$) and DOX (300 $\mu\text{g/mL}$) were incubated with OMVs (2×10^{10} particles) simultaneously at 37 $^\circ\text{C}$ for 2 h for co-loading. Excessive free drugs were removed by ultrafiltration (100 kDa) and washed with PBS three times. For the maximum drug loading capacity test, Ce6 was quantified by ultraviolet (UV) spectroscopy (660 nm, BlueStar A, Lab-Tech, China), DOX was quantified by Fluorescence Spectrometer (470/590 nm, RF-5301, Shimadzu, Japan).

Cumulative release of Ce6 and DOX from Ce6/DOX-OMVs was evaluated by using an ultrafiltration tube (100 kDa) against PBS (1/400, *v/v*). Laser-triggered release of OMVs from Ce6/DOX-OMVs@M was observed by TEM imaging. Laser-triggered (30 s) *in vitro* release of Ce6 and DOX from Ce6/DOX-OMVs@M were also quantified by UV spectroscopy and fluorescence spectroscopy.

2.8. *In vitro* cytotoxicity and ROS assay

We first investigated the cytotoxicity of OMVs co-loaded with Ce6 and DOX on macrophages. Raw264.7 macrophages seeded in 96-well plates were incubated with different OMV formulations at various concentrations. After 24 h of incubation, cell viability was assessed using the CCK-8 Assay (NCMBio, Soochow, China) by measuring the absorbance at 450 nm using an Infinite F50 microplate reader (Tecan, Switzerland). The concentration with high loading capacity but little influence in the viability of Raw264.7 macrophages were used for the further experiments. Calcein AM/PI Double Stain Kit (MKBio, Shanghai, China) was used to measure Ce6/DOX@OMVs-induced cell death. Raw264.7 macrophages were treated with various formulations containing Ce6 (2.5 $\mu\text{g/mL}$) or DOX (2.5 $\mu\text{g/mL}$) for 24 h. Cells were collected, washed with assay buffer three times and incubated with Calcein-AM (2 mM) and PI (1.5 mM) at 37 $^\circ\text{C}$ for 15 min, followed by observation under a fluorescence microscope to investigate cell death (red). Then, the *in vitro* cytotoxicity of Ce6/DOX-OMVs@M on 4T1 cells was evaluated by the CCK-8 assay. 4T1 cells (5×10^3 cells/well) seeded in 96-well plates were incubated with different formulations at various concentrations. After 24 h of incubation, cell viability was assessed using

the CCK-8 Assay. For formulations with Ce6, laser irradiation (660 nm, 5 mW/cm^2 , 2 min) was performed after 6 h of incubation. CCK-8 assay was performed for at least triplicate samples. For ROS assay, 4T1 cells were incubated with formulations similar to the *in vitro* cytotoxicity study with Ce6 (20 $\mu\text{g/mL}$). After 6 h of incubation and 2 min of laser irradiation. The generated ROS was measured by incubation with the DCFH-DA (Sigma-Aldrich, USA) at the concentration of 2 μM for 30 min. Fluorescence was observed under a microscope and quantified by the flow cytometry.

2.9. *In vivo* antitumor efficacy of Ce6/DOX-OMVs@M

Mice with orthotopic breast tumors were treated with PBS, Ce6, OMVs, DOX, Ce6@OMVs, DOX@OMVs, Ce6-OMVs@M, DOX-OMVs@M, or Ce6/DOX-OMVs@M two times via *i.v.* injection with an interval of four days. The injection dose was 100 μL and the concentration for free DOX and Ce6 were 1 mg/kg and 2 mg/kg, respectively. Laser irradiation (660 nm, 0.15 W/cm^2 , 10 min) was performed at the tumor site 24 h after injection. Bioluminescence images were obtained by IVIS Spectrum (PerkinElmer, USA). The bodyweight of mice was monitored every day. After the intervention, mice were sacrificed, tumors were excised and weighted. Blood was collected and levels of ALT, AST, BUN and Cr were analyzed. Lung and liver tissues were collected, imaged, fixed in 4% PFA, and stained with H&E. Tumors were stained by TUNEL and Ki67 immunohistochemistry to observe cell death and tumor proliferation.

2.10. Shifting macrophage polarization and inducing pyroptosis in the tumor by OMVs

Raw264.7 macrophages were seeded in a 6-well plate and treated with OMVs (1×10^{11} particles) or PBS for 6 h. Cells were imaged and washed with PBS. Then, cells were collected and cell suspension in PBS was added with 5 μL of PE Rat Anti-Mouse CD86 (BD Pharmingen, USA) for 15 min of incubation. Cells were collected and washed with PBS three times and detected by flow cytometry (BD, USA). For tumor-bearing mice treated with various formulations, tumors were collected, fixed, and sliced. Fluorescence immunohistochemistry was performed to evaluate macrophage polarization in tumors. Tumors were collected two days after treatments. Tumor tissues were fixed by 4% PFA and stained with fluorescence-labeled antibodies F4/80 (Servicebio, GB11027), CD86 (Servicebio, GB13585) and CD206 (Servicebio, GB113497).

In addition, flow cytometry analysis was performed to analyze the macrophages in the tumor microenvironment. After treatment, tumor-bearing mice were sacrificed and tumors collected. Tumors were cut into small tissue pieces and then digested with collagenase and DNase. Single-cell suspension were obtained by homogenizing tumor tissues in PBS. For macrophage analysis, cells were stained with CD45 (Biolegend, 103130), F4/80 (Biolegend, 123108), CD86 (Biolegend, 105011) and CD206 antibodies (Biolegend, 141706), and then analyzed by flow cytometry (CytoFLEX, Beckman Coulter, A00-1-1102).

For investigation of pyroptosis, 4T1 cells were incubated with OMVs for 6 h or 24 h. Cells were collected and the proteins were analyzed with sodium dodecyl sulfate-polyacrylamide gel electrophoresis (SDS-PAGE) and western blotting. Samples were incubated with Anti-Pro Caspase-1 (ab179515, Abcam, UK), Anti-GSDMD (ab209845, Abcam, UK), Anti-NLRP3 (ab263899, Abcam, UK) and Anti- β -actin (AF5001, Beyotime, China), followed by HRP-conjugated anti-rabbit IgG antibody (ZSGB-Bio, China). The protein expression was measured by a gel imaging system (ChemiDocTM Touch, Bio-Rad, USA). For mice with orthotopic 4T1 tumor, 24 h after OMV treatment, tumors were surgically excised and frozen by liquid nitrogen and stored at -80°C . Western blot was performed to evaluate the level of NLRP3, Caspase-1 and GSDMD protein level. qPCR was performed to analysis the mRNA level of NLRP3 (forward strand: 5'-GGAGTCTTCGCTGCTATGTACTA-3'; reverse

strand: 5'-GGACCTTCAGTCTCGGTTTC-3') and IL-1β (forward strand: 5'-TGGGAAACAACAGTGGTCAGG-3'; reverse strand: 5'-ATTAGAAA-CAGTCCAGCCATACTT-3') in tumor tissues. In addition, transcriptomic analysis (Novogene Co., Ltd., Beijing, China) was performed to further evaluate the pyroptosis-related mRNA level in tumor-bearing mice after treatment of OMVs for 24 h.

2.11. Hemolysis assay

The hemolysis activity of formulations was tested. Briefly, red blood

cells (RBCs) from whole blood of healthy BALB/c mice were collected and washed with saline for three times (1000 rpm, 10 min, 4 °C). Various formulations in normal saline were incubated with RBCs suspension at 37 °C for 1 h. Pure water was used as positive control while normal saline was used as negative control. The absorbance of the supernatants collected by centrifuging at 1000 g for 5 min from each group was measured using ultraviolet spectrophotometer (BlueStar A, Lab-Tech, China) at 545 nm. The hemolysis percentage (%) was calculated as $(A \text{ of samples} - A_0 \text{ negative control}) / (A_1 \text{ of positive control} - A_0 \text{ negative control}) \times 100\%$.

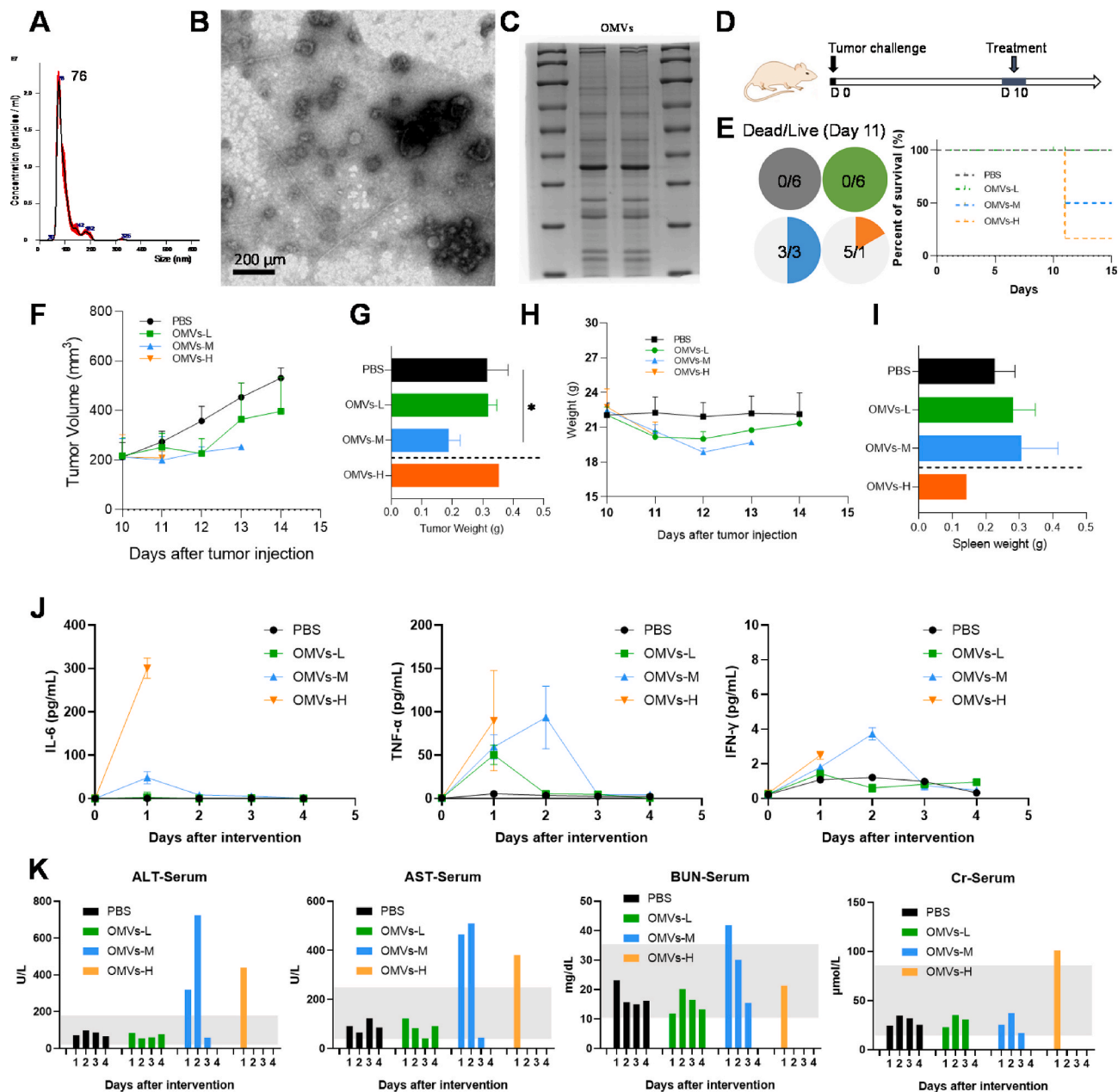


Fig. 1. Characterization, safety and antitumor potentials of OMVs. OMVs-L, OMVs-M and OMVs-H represent low (0.25×10^{12} particles), medium (0.50×10^{12} particles) and high (1.00×10^{12} particles) dose of OMVs respectively. (A) Size distribution of OMVs by nanoparticle tracking analysis; (B) Transmission microscope (TEM) image of OMVs; (C) Protein profiles of OMVs by Coomassie brilliant blue staining; (D) Treatment schedule of free OMVs against orthotopic breast tumor; (E) Survival of tumor-bearing mice after receiving OMVs treatment; (F) Tumor growth in mice receiving treatment of OMVs; (G) Tumor weight in mice after OMVs treatment, dot line indicate that the data for OMVs-H should not be compared to other groups as only one mice survived after OMVs-H injection, * $P < 0.05$; (H) Body weight of tumor-bearing mice before and after OMVs treatment; (I) Spleen weight in mice after OMVs treatment, dot line indicate that the data for OMVs-H should not be compared to other groups as only one mice survived after OMVs-H injection; (J) Analysis of serum levels of proinflammatory cytokines (IL-6, TNF-α and IFN-γ) in tumor-bearing mice after OMVs treatment; (K) Analysis serum levels of ALT, AST, BUN and Cr in tumor-bearing mice after OMVs treatment. Gray area indicates normal reference ranges.

2.12. Statistical analysis

Data were presented as the mean \pm SD. A two-tailed Student's *t*-test was applied to test the statistical significance of the difference between two groups, one-way analysis of variance (ANOVA) was applied to test the statistical significance of difference among three or more groups. The statistical significance was set at * $P < 0.05$, ** $P < 0.01$ and *** $P < 0.001$.

3. Results and discussion

3.1. OMVs preparation and characterization

OMVs were isolated from the culture medium of *E. coli* (DH5 α). OMVs were prepared by differential ultracentrifugation combined with ultrafiltration. The size of isolated OMVs was distributed mainly between 70 nm and 140 nm (Fig. 1A) by nanoparticle tracking analysis (NTA), and the polydispersed index (PDI) was 0.234. Transmission electronic microscope (TEM) images show the morphology of OMVs (Fig. 1B) and the particle size of OMVs under TEM matched with the results of NTA. The protein profile of isolated OMVs was characterized by Coomassie brilliant blue staining (Fig. 1C). The amount of lipopolysaccharide (LPS) in OMVs was quantified by endotoxin assay, and the yield was stable as similar levels of LPS in OMVs (0.65 ± 0.06 EU per 4×10^{12} OMV particles) was observed (Fig. S1).

3.2. Safety and antitumor potentials of OMVs

Safety has been a major concern for the use of OMVs for therapeutic purposes. Therefore, we firstly tested the therapeutic window and evaluated the safety and antitumor potential of different doses of free OMVs in mice with orthotopic TBNC (Fig. 1D). As a result, only one of six mice received *i.v.* injection of high dose of OMVs (OMVs-H: 1.00×10^{12} particles) survived, three of six mice received a medium dose of OMVs (OMVs-M: 0.50×10^{12} particles) survived, but all mice received a low dose of OMVs (OMVs-L: 0.25×10^{12} particles) survived (Fig. 1E). For the tumor growth, all three groups receiving OMVs treatment showed suppressed tumor growth (Fig. 1F) and decreased tumor weight (Fig. 1G). However, as only one mouse in the OMVs-H group survived, the data were not typically consistent with the dose-response relationship. Interestingly, we observed that the tumor turned to 'red' after OMVs treatment, but the phenomenon disappeared after two days and the tumor returned to normal color (Fig. S2). A similar phenomenon can be observed in tumor-bearing mice (Fig. S3A). Previous studies found that attenuated *Salmonella* can induce inflammation and thrombosis in tumors infected [22]. More importantly, it has been reported that *E. coli*-derived OMVs may promote intravascular coagulation through gasdermin D pathway [23]. Therefore, we assume that OMVs may trigger pro-inflammation and pro-thrombosis and turn the tumor 'red', but further investigation is required to reveal the underlying mechanism.

The bodyweight of tumor-bearing mice decreased sharply after OMVs injection for two days but recovered soon (Fig. 1H). The excised spleen (Fig. S3B) and their weight (Fig. 1I) showed that OMVs injection induced significant proliferation of spleen cells, which may be related to its immunostimulating effects. Also, as only one mouse in the OMVs-H group survived, the effect was not that significant. Those results demonstrated that free OMVs were highly toxic and have a very narrow therapeutic window, but the antitumor potential was also observed under controlled dose. Further, we evaluated the proinflammatory cytokines in tumor-bearing mice after OMVs injection. We observed that OMVs injection led to a significantly higher level of IL-6, TNF- α and INF- γ (Fig. 1J), and the effect can last for one to two days. Also, serum levels of ALT, AST, BUN and Cr demonstrated that OMVs-L was relatively safe with no increase of any of these indexes (Fig. 1K), OMV-M treatment slightly increased ALT, AST and BUN levels, but these indexes recovered

to normal reference ranges two days after injection. H&E staining of liver and spleen tissues showed that OMVs-M and OMVs-H may damage liver cells (Fig. S3B), but they can also induce proliferation of acini lienalis (Fig. S3B), further showing the immuno-stimulatory effect. These results indicated that OMVs have antitumor potentials by enhancing immunity, but a bioengineering strategy is required for enhancing its tumor-targeting ability and improving its safety and antitumor efficacy.

3.3. Preparation and characterization of OMVs@M

We used macrophage as the delivery vehicle as macrophage can be utilized as "Trojan Horse" vectors for nanoparticle delivery [24] and have innate phagocytic ability to exogenous particles such as OMVs [25]. Besides, it has been reported that OMVs may be able to lead M2-to-M1 polarization of macrophages for antitumor therapy [26], therefore facilitating targeted delivery of OMVs to the tumor site (Fig. 2A).

OMVs were loaded into macrophages by direct incubation. The loading of OMVs showed no damage, even if at a relatively high dose, to the cell viability of RAW 264.7 macrophages by CCK-8 assay (Fig. S4). The successful loading of OMVs into macrophages was confirmed by TEM images (Fig. 2B), Coomassie brilliant blue staining (Fig. 2C) and fluorescence microscope (Fig. 2D). Macrophages have a high loading capacity for OMVs and a single macrophage can handle and carry nearly 3×10^5 OMV particles as calculated by the endotoxin assay (Fig. S5).

In our study, murine Raw264.7 macrophages were used for the delivery of OMVs. However, it should be noted that Raw264.7 cell is the mouse mononuclear macrophage leukemia cell, which may cause the potential safety risks, such as leukemia. Therefore, Raw264.7 cell used in the current study is to demonstrate the delivery ability of macrophages in mice models and may not be suitable for clinical applications.

3.4. Macrophage migration and *in vivo* biodistribution

The fluorescence microscope of transwell macrophage migration assay showed more Pkh67-labeled macrophages in the lower chamber after 24 h (Fig. 2E), demonstrating that the loading of OMVs in Raw264.7 macrophages enhanced its migration from the upper chamber to 4T1 mammary tumor cells at the lower chamber (Fig. 2F). For *in vivo* biodistribution, OMVs@M successfully targeted the tumor site via *i.v.* injection (Fig. 2G), *ex vivo* fluorescence images also confirmed significant targeting ability of DiR-OMVs@M to the tumor, while free DiR and DiR-labeled OMVs showed no fluorescence at excised tumors (Fig. 2H). Besides, free OMVs showed the highest fluorescence intensity at the spleen but the lowest fluorescence intensity at other tissues (Fig. 2I), demonstrating that free OMVs, without macrophage-mediated delivery protection, would be cleared quickly during circulation after *i.v.* injection.

3.5. Improved safety and antitumor efficacy of OMVs@M

Following the dose of OMVs in our preliminary investigation, we prepared three different concentrations of OMVs@M (OMVs@M-L: 0.25×10^{12} OMV particles incubated with 1×10^6 macrophages; OMVs@M-M: 0.50×10^{12} OMV particles incubated with 2.5×10^6 macrophages; OMVs@M-H: 1.00×10^{12} OMV particles incubated with 3.5×10^6 macrophages) and evaluated its safety and antitumor efficacy (Fig. 3A). However, it should be noted that the number of OMV particles in OMVs@M may not be the same as incubated, because OMVs may not be intact within macrophages after phagocytosis. For survival, all tumor-bearing mice receiving OMVs@M-L and OMVs@M-M survived after *i.v.* injection; however, three of six mice receiving OMVs@M-H died the day after injection (Fig. 3B). For the tumor growth, OMVs@M-L, OMVs@M-M and OMVs@M-H showed similar suppressing effects on the tumor growth (Fig. 3C). OMVs@M-M group showed the lowest

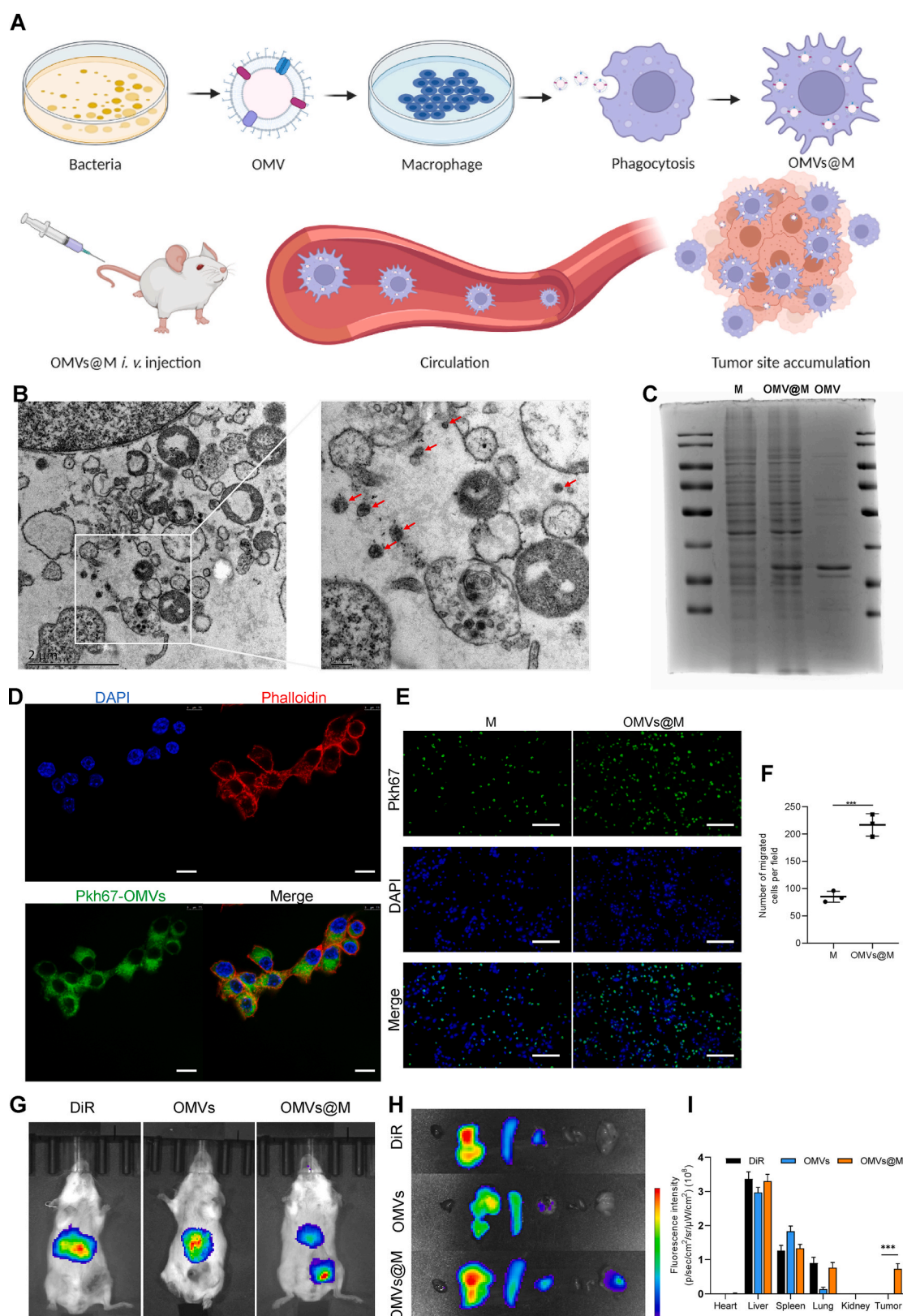


Fig. 2. Design, development, characterization and tumor-targeting of OMVs-loaded macrophage (OMVs@M). (A) Illustration for the development of OMVs@M for tumor targeting and therapy; (B) TEM images of OMVs@M highlighting the loading of OMVs in macrophage; (C) Protein profiles of OMVs@M by Coomassie brilliant blue staining showing the loading of OMVs in macrophage; (D) Confocal fluorescence microscopy images showing the loading of Pkh67-labeled OMVs in macrophages. Scale bar = 10 μm. (E) Transwell assay showing the migration of macrophage and OMVs@M (upper chamber) to 4T1 tumor cells (lower chamber) Scale bar = 100 μm. (F) Quantification of migrated macrophages in the lower chamber; (G) In vivo biodistribution of DiR-labeled OMVs and OMVs@M in mice with orthotopic breast tumor 8 h after injection; (H) Ex vivo biodistribution of DiR-labeled OMVs and OMVs@M in tumors and major organs 8 h after injection; (I) Quantification of fluorescence intensity in tumors and major organs. ****P* < 0.001.

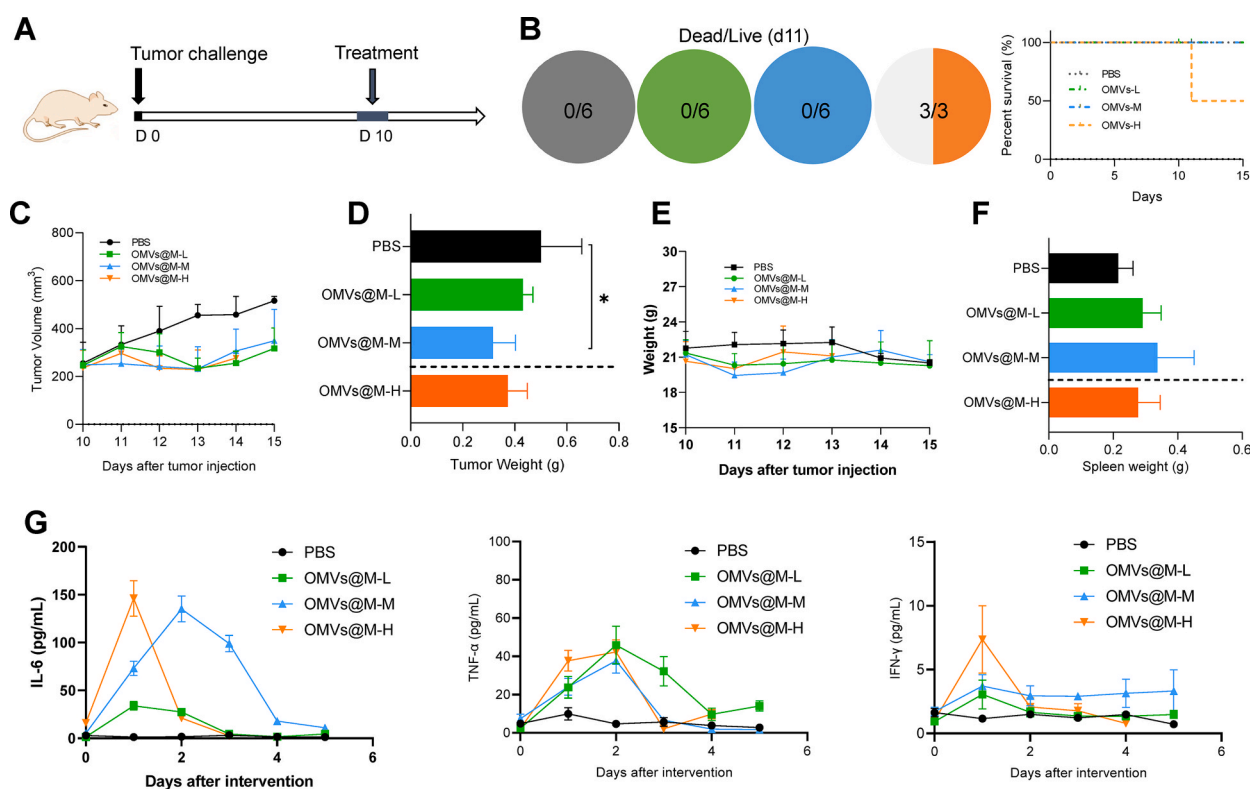


Fig. 3. Safety and antitumor efficacy of OMVs@M (OMVs@M-L, OMVs@M-M, OMVs@M-H). OMVs@M-L: 0.25×10^{12} particles/ 1×10^6 M cells; OMVs@M-M: 0.50×10^{12} particles/ 2.5×10^6 M cells; OMVs@M-H: 1.00×10^{12} particles/ 3.5×10^6 M cells. (A) Treatment schedule of OMVs@M against orthotopic breast tumor; (B) Survival of tumor-bearing mice receiving OMVs@M treatment; (C) Tumor growth in mice receiving treatment of OMVs@M; (D) Tumor weight in mice after OMVs@M treatment, dot line indicate that the data for OMVs@M-H should not be compared to other groups as only one mice survived after OMVs@M-H injection; (E) Body weight of tumor-bearing mice before and after OMVs@M treatment; (F) Spleen weight in mice after OMVs@M treatment, dot line indicate that the data for OMVs@M-H should not be compared to other groups as only a half mice survived after OMVs@M-H injection; (G) Analysis of serum levels of proinflammatory cytokines (IL-6, TNF- α and IFN- γ) in tumor-bearing mice after OMVs@M treatment. * $P < 0.05$.

weight of excised tumors (Fig. 3D). Tumors were also turned ‘red’ for one day for all three OMVs@M groups (Fig. S6A), and images of tumor-bearing mice showed the ‘red’ phenomenon of tumors after OMVs@M injection (Fig. S7). The decreasing trend of body weight of tumor-bearing mice was mild and the bodyweight recovered very soon for all groups (Fig. 3F), suggesting improved safety of OMVs@M than free OMVs. The excised spleen (Fig. 3G) and their weight (Fig. 3H) showed that OMVs@M injection can also induce the proliferation of spleen cells. Similarly, as half mice in the OMVs@M-H group died, the observed antitumor efficacy and the proliferation of spleen cells were not that significant as OMVs@M-M. Also, we evaluated the level of proinflammatory cytokines in tumor-bearing mice after OMVs@M injection. OMVs@M injection led to a higher level of IL-6, TNF- α and IFN- γ (Fig. 3I), and the effect can last for two to three days, longer than the effect of free OMVs (Figure 1L). These results indicated macrophage-mediated delivery of OMVs improved safety while maintaining its antitumor potency. More importantly, the OMVs@M-M showed the optimal therapeutic efficacy with high tolerability, providing a platform with a suitable therapeutic window for further evaluation and improvement.

3.6. Development and characterization of Ce6/DOX-OMVs@M

To further improve the antitumor efficacy of OMVs@M, we encapsulated photosensitizer Ce6 and chemotherapeutic drug doxorubicin (DOX) into OMVs for laser-triggered release and synergic antitumor therapy before loading into macrophages (Fig. 4A).

Ce6 and DOX were co-incubated with OMVs to produce Ce6/DOX-OMVs, and the maximum loading capacity was $31.44 \pm 5.21 \mu\text{g}$ and

$41.92 \pm 4.86 \mu\text{g}$ per 1×10^{11} OMV particles for Ce6 and DOX respectively (Fig. S8A). We performed the endotoxin assay to quantify the LPS level in Ce6/DOX-OMVs@M and the calculated dose of Ce6 and DOX in Ce6/DOX-OMVs@M were $4.37 \pm 0.52 \mu\text{g}$ and $2.54 \pm 0.21 \mu\text{g}$ per 10^6 Raw 264.7 cells, respectively (Fig. S9). The loading of Ce6 and DOX by incubation did not affect significantly the size of OMVs (Fig. S10). For drug release profiles, both Ce6 and DOX showed controlled release from Ce6/DOX-OMVs. During 24 h of release, about 15% of DOX and 8% of Ce6 were released from Ce6/DOX-OMVs, but the releasing trend was similar (Fig. S8B). Laser-triggered release of OMVs from Ce6/DOX-OMVs@M can be observed by TEM imaging (Fig. 4B). Induced by laser irradiation, Ce6/DOX-OMVs@M showed multiple holes, from where OMVs were released. Laser-triggered release of Ce6 and DOX from Ce6/DOX-OMVs@M were quantified by ultraviolet spectroscopy and fluorescence spectroscopy and a burst release was observed after turning on the laser for a very short period (Fig. 4C). At resting conditions, less than 10% of DOX and Ce6 were released from Ce6/DOX-OMVs@M; however, about 80% of DOX and 70% of Ce6 were released quickly in response to laser irradiation (Fig. 4C), demonstrating successful laser-triggered release abilities of Ce6/DOX-OMVs@M. A similar photo-responsive phenomenon has also been reported in previous reports [27–29]. Light irradiation can achieve on-demand drug release by rupturing the membrane of vesicles via generation of singlet oxygen and phospholipids oxidation [30,31]. It has been reported that the NIR irradiation may also marginally increase the temperature [32]. However, substantial increase of the temperature requires continuous irradiation for at least several minutes. When testing the triggered release, we only used irradiation for 30 s. Therefore, the release of incorporated drugs is expected to mainly through the laser-activation

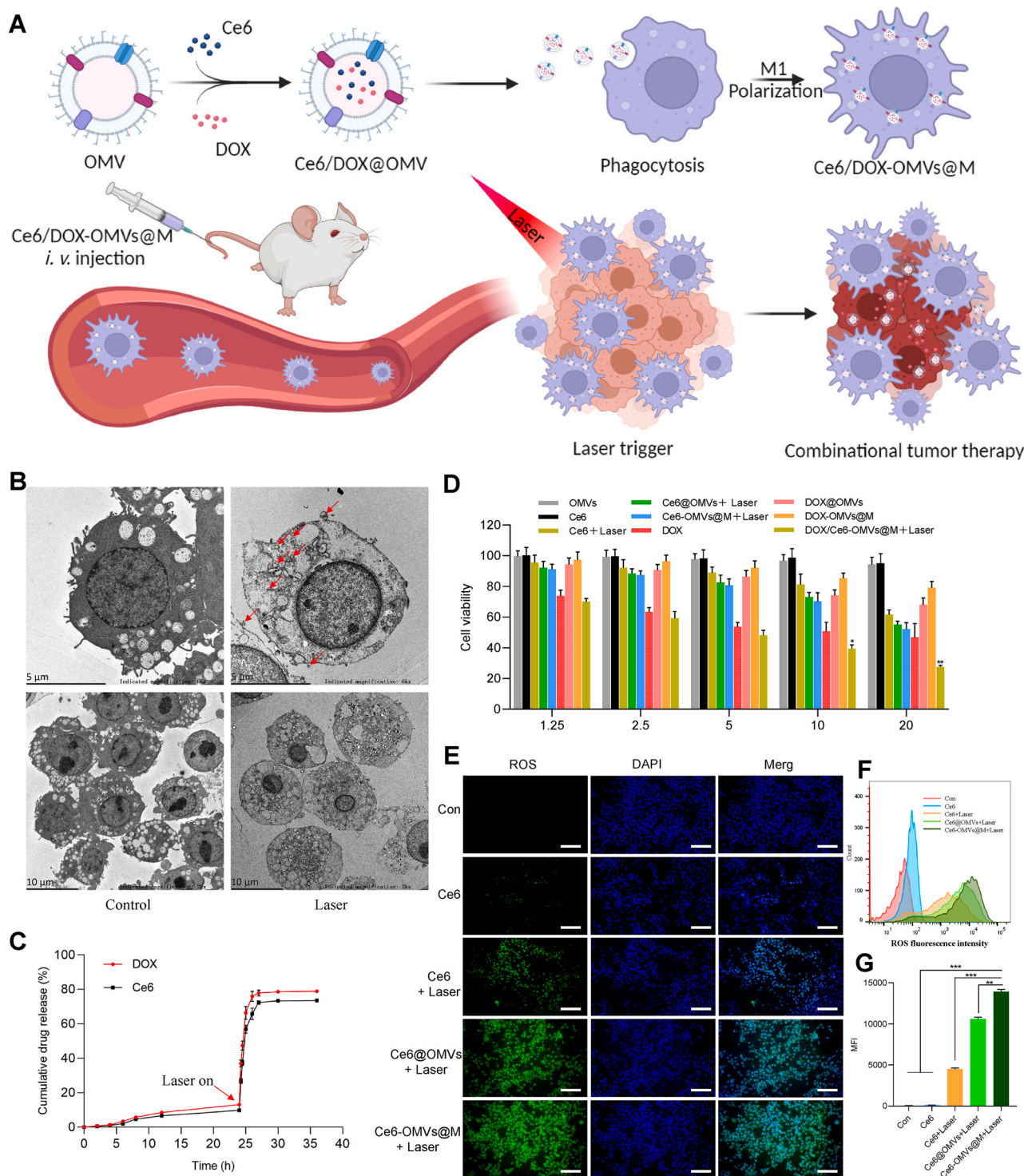


Fig. 4. Design and characterization of DOX/Ce6-OMVs@M. (A) Design of DOX/Ce6-OMVs@M for laser-triggered release and combined photodynamic/chemo-immunotherapy of tumor. (B) TEM images of DOX/Ce6-OMVs@M with or without laser irritation, laser-triggered release of OMVs were highlighted by red arrows; (C) Cumulative release of DOX and Ce6 from OMVs before and after laser irradiation; (D) In vitro cytotoxicity of DOX/Ce6-OMVs@M by CCK8 assay; (E) Fluorescence images showing the generation of ROS in 4T1 tumor cells after incubation with DOX/Ce6-OMVs@M, scale bar = 100 μ m; (F) ROS fluorescence intensity of 4T1 tumor cells by flow cytometry; (G) Quantitative analysis of ROS fluorescence intensity by flow cytometry. ** $P < 0.01$, *** $P < 0.001$.

but not temperature change.

3.7. In vitro cytotoxicity and reactive oxygen species (ROS) assay

The cytotoxicity of OMVs co-loaded with Ce6 and DOX on Raw264.7 macrophages was assessed by the CCK-8 assay and the Calcein AM/PI

Double Staining. Ce6 and Ce6@OMVs showed minimal influence in the viability of macrophages, free DOX decreased the cell viability at relatively low concentration, and DOX@OMVs and Ce6/DOX@OMVs decreased the cell viability only at relatively high concentration (Fig. S11), demonstrating that the encapsulation by OMVs significantly decreased the cytotoxicity of DOX on macrophages. Further, at the given

concentration of DOX (2.5 µg/mL), significant cell death can be observed under the fluorescence microscope by Calcein-AM and PI staining for free DOX treatment but other groups including free OMVs, ce6, Ce6@OMVs, DOX@OMVs and Ce6/DOX@OMVs showed minimal damage to the macrophage carrier (Fig. S12). Those results demonstrated that OMVs co-loaded with Ce6 and DOX would not affect the viability of macrophages as vectors.

The cytotoxicity of Ce6/DOX-OMVs@M on 4T1 tumor cells was evaluated firstly by the CCK-8 assay. Ce6/DOX-OMVs@M plus laser irradiation lead to the most significant tumor cell death for all concentrations (Fig. 4D). Further, we assessed the generation of ROS by Ce6/DOX-OMVs@M as it has been reported that photodynamic therapy can induce therapeutic ROS and trigger immunogenic cell death (ICD) [33–35]. As observed by fluorescence microscope, Ce6, Ce6@OMVs and Ce6-OMVs@M effectively induced ROS generation in response to laser irradiation (Fig. 4E). Flow cytometry and the quantitative analysis of fluorescence intensity in 4T1 tumor cells showed that Ce6-OMVs@M treatment produced the most significant generation of ROS in 4T1 tumor cells (Fig. 4F and G). Those results demonstrated that the development of Ce6/DOX-OMVs@M enhanced remarkably the antitumor efficacy of OMVs.

3.8. *In vivo* antitumor efficacy of Ce6/DOX-OMVs@M

The dose of OMVs@M-M with potent antitumor efficacy and high safety was slightly modified (0.25×10^{12} OMV particles incubated with 2.5×10^6 macrophages) and then used for the *in vivo* evaluation of Ce6/DOX-OMVs@M. Mice with orthotopic breast tumors were intravenously administrated with various formulations for two times with an interval of four days (Fig. 5A). Bioluminescence images and the tumor volume in mice were monitored. Free Ce6, OMVs and DOX, with a relatively low dose, showed minimal therapeutic effects against tumor growth as compared to the PBS control group (Fig. 5B and C). Ce6@OMVs and DOX@OMVs suppressed tumor growth during the treatment but the tumor rebounded soon after the treatment was discontinued (Fig. 5B and C), Ce6-OMVs@M and DOX-OMVs@M showed better antitumor effects as compared to Ce6@OMVs and DOX@OMVs for the enhanced tumor-targeting ability, but the tumor growth also showed a rebound trend after treatment was discontinued (Fig. 5C and D), despite that the tumor in several mice receiving Ce6-OMVs@M injection was eradicated without recurrence (Fig. 5B and E). For the Ce6/DOX-OMVs@M group, the treatment inhibited effectively the tumor growth and most tumors were eradicated after treatment (Fig. 5B, C, 5E, 5F). It should be noted that while the tumor was eradicated in mice, the wound at the tumor site after laser irradiation remained for several days (Fig. 5B) making it difficult to manually measure the tumor volume (Fig. 5D). But no bioluminescence of tumor cells can be detected (Fig. 5B) and no solid tumor can be excised by surgery (Fig. 5E).

When Ce6/DOX-OMVs@M reached tumor site, it is speculated that Ce6/DOX-OMVs would be released from macrophages upon later irritation and then uptake by surrounding cells with in the tumor micro-environment, inducing synergic antitumor effects. The released chemotherapeutics may also damage vehicle macrophages, but the immunostimulating activity of OMVs would eventually lead to enhanced antitumor responses.

The body weight of tumor-bearing mice decreased after receiving treatments containing OMVs but recovered soon after the treatment (Fig. S13). Moreover, we evaluated the lung metastasis in mice after treatment as 4T1 tumors were highly metastatic to the lung. From the lung tissues imaged (Fig. 5G) and stained with H&E (Fig. 5H), it can be observed that the number of the metastatic site at the lung was consistent with the tumor growth. The PBS group showed multiple lung metastatic sites and no metastasis can be observed for the Ce6/DOX-OMVs@M group (Fig. 5H).

The hepatotoxicity of Ce6/DOX-OMVs@M was evaluated as significant accumulation was observed in the biodistribution study. As a result,

H&E staining of the liver tissue showed no abnormal changes (Fig. S14) and serum levels of ALT and AST were within normal range (Fig. S15). Also, the serum levels of BUN and Cr showed no significant change to kidney functions after the Ce6/DOX-OMVs@M treatment (Fig. S15). Further, we tested the hemolysis activity of formulations. The result showed that none of the formulation at the same concentration for injection significantly increased (<5%) the hemolysis of RBC after incubation (Fig. S16). Collectively, these results demonstrated the safety of Ce6/DOX-OMVs@M.

Macrophages are one of the major cell types in lung and is responsible for clearing debris through phagocytosis [36]. The lung tissues stained with H&E were also carefully evaluated after Ce6/DOX-OMVs@M administration, and no pathological change was observed in the lung. In addition, macrophage-based biomimetic delivery systems have been previously used for lung delivery and pulmonary diseases treatment [37,38], and the therapeutic effects are prominent. Therefore, while the developed Ce6/DOX-OMVs@M therapeutic platform was larger than nanoparticles, it would not affect the pulmonary functions.

For TdT-mediated dUTP Nick-End Labeling (TUNEL) and Ki67 immunochemistry of tumor tissues, the most significant cell death (Fig. 5I) and suppressed tumor cell proliferation (Fig. 5J) were observed for the Ce6/DOX-OMVs@M group. Those results demonstrated superior antitumor efficacy of Ce6/DOX-OMVs@M combining multiple therapeutic strategies.

The hemolysis assay results showed that Ce6/DOX-OMVs@M are highly comparable and would not result in hemolysis (Fig. S16), demonstrating that Ce6/DOX-OMVs@M would be nontoxic toward RBCs after *i.v.* administration.

3.9. Potential antitumor mechanisms of OMVs

To explore the antitumor mechanisms of OMVs, we firstly evaluated the effect of OMVs on shifting macrophage polarization *in vitro*. It can be observed that the morphology of Raw264.7 macrophages changed from round to mixed morphology, with both fibroblast-like shape and round shape, after incubation with OMVs for 24 h (Fig. 6A). Flow cytometry analysis revealed that OMVs can induce activation of macrophages from naïve to M1 type (CD86⁺) after incubation for 6 h (Fig. 6B and C). Previous studies also reported that LPS treatment can activate mitogen-activated protein kinases in Raw264.7 macrophages and induce morphological changes [39]. More importantly, in tumor tissues, it can be observed that the level of M1-like macrophage was significantly higher in mice receiving treatment containing OMVs (Fig. 6D), and the M1-like phenotype is associated with the antitumor effects [40]. Further, we analyzed the macrophages in tumors by flow cytometry. Elevated level of M1-like macrophages and M1/M2 ratios was observed in mice receiving treatment containing OMVs and especially for Ce6/DOX-OMVs@M treatment (Fig. 6E), demonstrating beneficial M2-to-M1 polarization ability of OMVs and the therapeutic platform. It worth mention that inflammatory cytokine levels in the tumor may also reflect the phenotype as macrophages are major source of inflammatory cytokines. However, inflammatory cytokines can also be produced by other cells such as lymphocytes, fibroblast and endothelial cells in the tumor microenvironment. Besides, cytokines levels may not directly reflect the phenotype of macrophages. We therefore did not investigate the inflammatory cytokines in the tumor for characterization of macrophage polarization. This would not affect the immunohistochemistry (Fig. 6D) and flow cytometry (Fig. 6E) results. Overall, the antitumor effects of OMVs may result from their ability to activate macrophages and shift M2-to-M1 polarization at the tumor site.

A major component of OMVs, LPS, is also a classical inducer of pyroptosis [41]. Pyroptosis has shown antitumor potentials by activating immunity [42]. We therefore evaluated whether OMVs can activate pyroptosis in tumors. As a result, 4T1 tumor cells incubated with OMVs showed a significantly higher level of NLRP3, cleaved

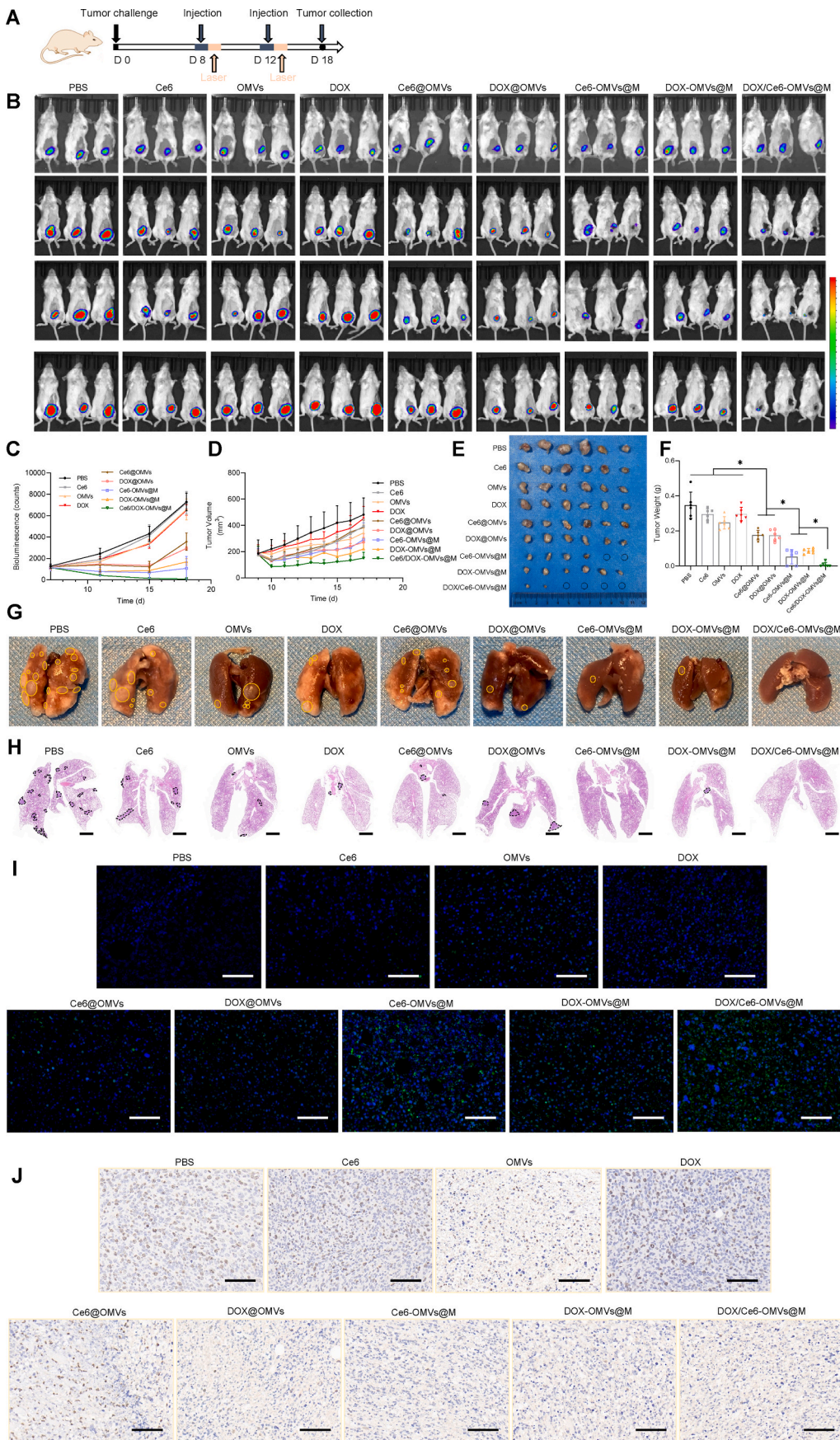
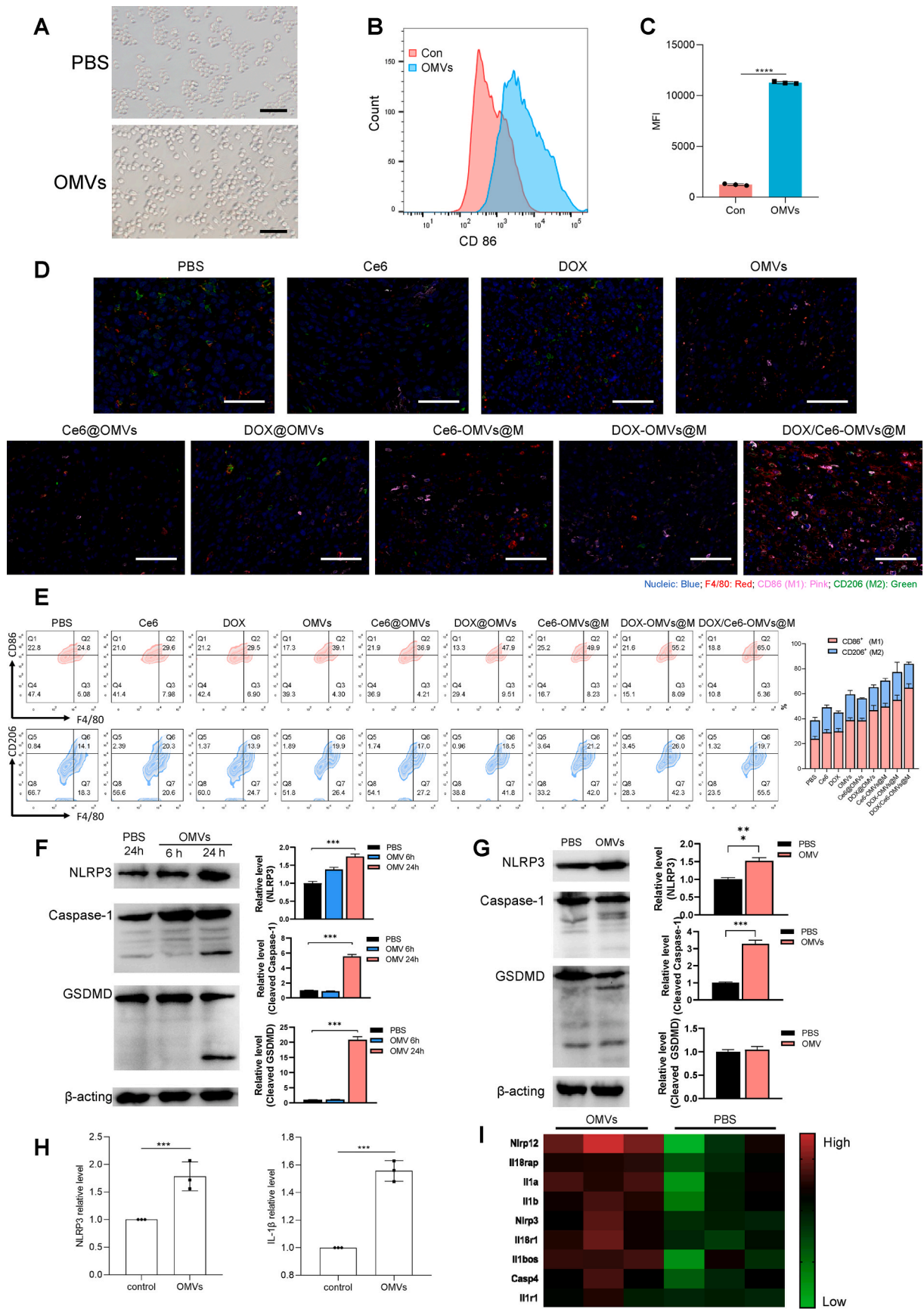


Fig. 5. Antitumor efficacy of DOX/Ce6-OMVs@M against orthotopic TNBC in mice; (B) Bioluminescence images of tumor-bearing mice before and after treatment. (C) Quantitative analysis of bioluminescence intensity at the tumor site. (D) Tumor growth in mice before and after treatment. (E) Images of excised tumors after treatment, black circle indicate the tumor was eradicated; (F) Weight of excised tumor after treatment; (G) Images of lung in tumor-bearing mice after treatment, metastasis sites were highlighted by yellow circle; (H) H&E staining of lung tissues in tumor-bearing mice after treatment, metastasis site were highlighted by black dotted lines. Scale bar = 2 mm. (I) TUNEL-stained 4T1 tumors after treatment. Scale bar = 100 μ m. * P < 0.05.



(caption on next page)

Fig. 6. Potential mechanisms of OMVs for antitumor effects by shifting macrophage polarization and inducing pyroptosis. (A) Images of Raw264.7 macrophages treated with PBS or OMVs, changes of morphology of OMVs-treated cells can be observed, scale bar = 100 μm ; (B) Flow cytometry showing the level of CD86 (M1 marker) in macrophages incubated with OMVs; (C) Quantitative analysis of fluorescence intensity of CD86 in macrophage incubated with OMVs, Raw264.7 macrophages treated with OMVs showed elevated expression of CD86. (D) Fluorescence immunochemistry of 4T1 tumors after treatment of various types of formulations with or without OMVs, scale bar = 100 μm . (E) Flow cytometry analysis of macrophages in tumors after treatment. (F) Western blot showing the activation of pyroptosis in 4T1 cells by OMVs *in vitro*, levels of cleaved Caspase-1 and GSDMD were quantified and compared; (G) Western blot showing the activation of pyroptosis in 4T1 tumors by OMVs *in vivo*, levels of cleaved Caspase-1 and GSDMD were quantified and compared; (H) qPCR analysis of NLRP3 and IL-1 β levels in 4T1 cells after incubation with PBS or OMVs; (I) Transcriptomic analysis showing the activation of pyroptosis-related mRNA in tumors by OMVs. **** $p < 0.001$.

Caspase-1 and cleaved GSDMD both *in vitro* (Fig. 6F) and *in vivo* (Fig. 6G); the qPCR results also demonstrated high levels of NLRP3 and IL-1 β mRNA in 4T1 tumors treated with OMVs (Fig. 6H). Further, the transcriptomic analysis identified elevated pyroptosis-related mRNA including NLRP3, IL1 β , caspase-4 and NLRP12 (Fig. 6I). Collectively, these results demonstrated that the potential mechanisms for the antitumor effects of OMVs may be associated with its ability to activate macrophage to M1-like phenotype and induce pyroptosis in tumor cells.

4. Conclusion

In this study, we demonstrated that OMVs can be used as immunostimulating agents to enhance antitumor immunity, but the narrow therapeutic window of free OMVs limited its application. To improve the safety and the antitumor efficacy of OMVs, we loaded OMVs into macrophages and explored OMVs as platforms for co-delivery of Ce6 and DOX for combinational tumor photodynamic/chemo-/immunotherapy. The developed Ce6/DOX-OMVs@M showed high safety and eradicated orthotopic TNBC in mice and prevented tumor metastasis. Our mechanism studies showed that OMVs could shift tumor-associated macrophage M2-to-M1 polarization and activate pyroptosis-related pathways to activate antitumor immune responses. The presented work demonstrates OMVs are promising immunotherapeutic agents and can be used as platforms in combination with other strategies for synergic antitumor therapy.

CRedit authorship contribution statement

Yongjiang Li: Conceptualization, Methodology, Software, Data curation, Validation, Visualization, Writing – original draft, Writing – review & editing. **Junyong Wu:** Conceptualization, Methodology, Software, Data curation, Formal analysis. **Xiaohan Qiu:** Methodology. **Suhe Dong:** Formal analysis. **Jun He:** Formal analysis. **Jihua Liu:** Data curation. **Wenjie Xu:** Data curation. **Si Huang:** Methodology, Data curation. **Xiongbin Hu:** Supervision, Data curation. **Da-Xiong Xiang:** Conceptualization, Resources, Project administration, Supervision, Funding acquisition.

Declaration of competing interest

The authors declare no conflict of interest.

Acknowledgments

This work was supported by the Hunan Provincial Science and Technology Plan (No. 2016TP2002).

Appendix A. Supplementary data

Supplementary data to this article can be found online at <https://doi.org/10.1016/j.bioactmat.2022.05.037>.

References

- [1] H. Sung, J. Ferlay, R.L. Siegel, M. Laversanne, I. Soerjomataram, A. Jemal, F. Bray, Global cancer statistics 2020: GLOBOCAN estimates of incidence and mortality worldwide for 36 cancers in 185 countries, *CA Cancer J. Clin.* 71 (2021) 209–249.
- [2] L. Yin, J.J. Duan, X.W. Bian, S.C. Yu, Triple-negative breast cancer molecular subtyping and treatment progress, *Breast Cancer Res.* 22 (2020) 61.
- [3] Y. Yang, Cancer immunotherapy: harnessing the immune system to battle cancer, *J. Clin. Invest.* 125 (2015) 3335–3337.
- [4] D.M. Pardoll, The blockade of immune checkpoints in cancer immunotherapy, *Nat. Rev. Cancer* 12 (2012) 252–264.
- [5] R.M. Pearson, L.M. Casey, K.R. Hughes, S.D. Miller, L.D. Shea, *In vivo* reprogramming of immune cells: technologies for induction of antigen-specific tolerance, *Adv. Drug Deliv. Rev.* 114 (2017) 240–255.
- [6] A. Marra, G. Viale, G. Curigliano, Recent advances in triple negative breast cancer: the immunotherapy era, *BMC Med.* 17 (2019) 90.
- [7] T.E. Keenan, S.M. Tolaney, Role of immunotherapy in triple-negative breast cancer, *J. Natl. Compr. Cancer Netw.* 18 (2020) 479–489.
- [8] W.B. Coley, Treatment of inoperable malignant tumors with the toxins of erysipelas and the bacillus prodigiosus. 1, *Am. J. Med. Sci.* 108 (1894) 50, 1827–1924.
- [9] Z. Li, Y. Wang, J. Liu, P. Rawding, J. Bu, S. Hong, Q. Hu, Chemically and biologically engineered bacteria-based delivery systems for emerging diagnosis and advanced therapy, *Adv. Mater.* 33 (2021), e2102580.
- [10] J. Wang, M. Zhu, G. Nie, Biomembrane-based nanostructures for cancer targeting and therapy: from synthetic liposomes to natural biomembranes and membrane-vesicles, *Adv. Drug Deliv. Rev.* 178 (2021), 113974.
- [11] S. Wang, J. Gao, Z. Wang, Outer membrane vesicles for vaccination and targeted drug delivery, *Wiley Interdiscip. Rev. Nanomed. Nanobiotechnol.* 11 (2019) e1523.
- [12] C. Irene, L. Fantappiè, E. Caproni, F. Zerbini, A. Anesi, M. Tomasi, I. Zanella, S. Stupia, S. Prete, S. Valensin, Bacterial outer membrane vesicles engineered with lipidated antigens as a platform for *Staphylococcus aureus* vaccine, *Proc. Natl. Acad. Sci. U S A.* 116 (2019) 21780–21788.
- [13] E.A. Semchenko, A. Tan, R. Borrow, K.L. Seib, The serogroup B meningococcal vaccine Bexsero elicits antibodies to *Neisseria gonorrhoeae*, *Clin. Infect. Dis.* 69 (2019) 1101–1111.
- [14] O.Y. Kim, H.T. Park, N.T.H. Dinh, S.J. Choi, J. Lee, J.H. Kim, S.-W. Lee, Y.S. Gho, Bacterial outer membrane vesicles suppress tumor by interferon- γ -mediated antitumor response, *Nat. Commun.* 8 (2017) 626.
- [15] D. Yang, S.Y. Park, Y.S. Park, H. Eun, S.Y. Lee, Metabolic engineering of *Escherichia coli* for natural product biosynthesis, *Trends Biotechnol.* 38 (2020) 745–765.
- [16] L.P. Jahromi, G. Fuhrmann, Bacterial extracellular vesicles: understanding biology promotes applications as nanopharmaceuticals, *Adv. Drug Deliv. Rev.* 173 (2021) 125–140.
- [17] Z. Cao, J. Liu, Bacteria and bacterial derivatives as drug carriers for cancer therapy, *J. Contr. Release* 326 (2020) 396–407.
- [18] S.M. Toor, V. Sasidharan Nair, J. Decock, E. Elkord, Immune checkpoints in the tumor microenvironment, *Semin. Cancer Biol.* 65 (2020) 1–12.
- [19] B.W. Simpson, M.S. Trent, Pushing the envelope: LPS modifications and their consequences, *Nat. Rev. Microbiol.* 17 (2019) 403–416.
- [20] W. Huang, Q. Zhang, W. Li, M. Yuan, J. Zhou, L. Hua, Y. Chen, C. Ye, Y. Ma, Development of novel nanoantibiotics using an outer membrane vesicle-based drug efflux mechanism, *J. Contr. Release* 317 (2020) 1–22.
- [21] Y.J. Li, J.Y. Wu, X.B. Hu, T. Ding, T. Tang, D.X. Xiang, Biomimetic liposome with surface-bound elastase for enhanced tumor penetration and chemo-immunotherapy, *Adv. Healthc. Mater.* 10 (2021), e2100794.
- [22] X. Yi, H. Zhou, Y. Chao, S. Xiong, J. Zhong, Z. Chai, K. Yang, Z. Liu, Bacteria-triggered tumor-specific thrombosis to enable potent photothermal immunotherapy of cancer, *Sci. Adv.* 6 (2020) eaba3546.
- [23] Y. Peng, M. Gao, Y. Liu, X. Qiu, X. Cheng, X. Yang, F. Chen, E. Wang, Bacterial outer membrane vesicles induce disseminated intravascular coagulation through the caspase-11-gasdermin D pathway, *Thromb. Res.* 196 (2020) 159–166.
- [24] Y. Qi, X. Yan, T. Xia, S. Liu, Use of macrophage as a Trojan horse for cancer nanotherapeutics, *Mater. Des.* 198 (2021), 109388.
- [25] Q. Guo, X. Li, W. Zhou, Y. Chu, Q. Chen, Y. Zhang, C. Li, H. Chen, P. Liu, Z. Zhao, Y. Wang, Z. Zhou, Y. Luo, C. Li, H. You, H. Song, B. Su, T. Zhang, T. Sun, C. Jiang, Sequentially triggered bacterial outer membrane vesicles for macrophage metabolism modulation and tumor metastasis suppression, *ACS Nano* 15 (2021) 13826–13838.
- [26] S. Qing, C. Lyu, L. Zhu, C. Pan, S. Wang, F. Li, J. Wang, H. Yue, X. Gao, R. Jia, W. Wei, G. Ma, Biomimetic bacterial outer membrane vesicles potentiate safe and efficient tumor microenvironment reprogramming for anticancer therapy, *Adv. Mater.* 32 (2020), e2002085.
- [27] D. Wu, S. Xu, X. Zhang, Y. Li, W. Zhang, Q. Yan, Q. Yang, F. Guo, G. Yang, A near-infrared laser-triggered size-shrinkable nanosystem with *in situ* drug release for deep tumor penetration, *ACS Appl. Mater. Interfaces* 13 (2021) 16036–16047.

- [28] J. Su, H. Sun, Q. Meng, Q. Yin, P. Zhang, Z. Zhang, H. Yu, Y. Li, Bioinspired nanoparticles with NIR-controlled drug release for synergetic chemophotothermal therapy of metastatic breast cancer, *Adv. Funct. Mater.* 26 (41) (2016) 7495–7506.
- [29] Q. Pei, X. Hu, X. Zheng, S. Liu, Y. Li, X. Jing, Z. Xie, Light-activatable red blood cell membrane-camouflaged dimeric prodrug nanoparticles for synergistic photodynamic/chemotherapy, *ACS Nano* 12 (2018) 1630–1641.
- [30] J. Ding, G. Lu, W. Nie, L.L. Huang, Y. Zhang, W. Fan, G. Wu, H. Liu, H.Y. Xie, Self-Activatable photo-extracellular vesicle for synergistic trimodal anticancer therapy, *Adv. Mater.* 33 (2021), e2005562.
- [31] A.Y. Rwei, J.J. Lee, C. Zhan, Q. Liu, M.T. Ok, S.A. Shankarappa, R. Langer, D. S. Kohane, Repeatable and adjustable on-demand sciatic nerve block with phototriggerable liposomes, *Proc. Natl. Acad. Sci. U. S. A.* 112 (2015) 15719–15724.
- [32] V.D. Nguyen, H.K. Min, D.H. Kim, C.S. Kim, J. Han, J.O. Park, E. Choi, Macrophage-mediated delivery of multifunctional nanotherapeutics for synergistic chemo-photothermal therapy of solid tumors, *ACS Appl. Mater. Interfaces* 12 (2020) 10130–10141.
- [33] W. Li, J. Yang, L. Luo, M. Jiang, B. Qin, H. Yin, C. Zhu, X. Yuan, J. Zhang, Z. Luo, Targeting photodynamic and photothermal therapy to the endoplasmic reticulum enhances immunogenic cancer cell death, *Nat. Commun.* 10 (2019) 3349.
- [34] H. Wang, K. Wang, L. He, Y. Liu, H. Dong, Y. Li, Engineering antigen as photosensitizer nanocarrier to facilitate ROS triggered immune cascade for photodynamic immunotherapy, *Biomaterials* 244 (2020), 119964.
- [35] A. Gao, B. Chen, J. Gao, F. Zhou, M. Saeed, B. Hou, Y. Li, H. Yu, Sheddable prodrug vesicles combating adaptive immune resistance for improved photodynamic immunotherapy of cancer, *Nano Lett.* 20 (2020) 353–362.
- [36] S. He, J. Gui, K. Xiong, M. Chen, H. Gao, Y. Fu, A roadmap to pulmonary delivery strategies for the treatment of infectious lung diseases, *J. Nanobiotechnol.* 20 (2022) 101.
- [37] X. Sang, Y. Wang, Z. Xue, D. Qi, G. Fan, F. Tian, Y. Zhu, J. Yang, Macrophage-targeted lung delivery of dexamethasone improves pulmonary fibrosis therapy via regulating the immune microenvironment, *Front. Immunol.* 12 (2021), 613907.
- [38] M. Evangelopoulos, I.K. Yazdi, S. Acciaro, R. Palomba, F. Giordano, A. Pasto, M. Sushnitha, J.O. Martinez, N. Basu, A. Torres, S. Hmaidan, A. Parodi, E. Tasciotti, Biomimetic cellular vectors for enhancing drug delivery to the lungs, *Sci. Rep.* 10 (2020) 172.
- [39] E.J. Kim, M.Y. Lee, Y.J. Jeon, Silymarin inhibits morphological changes in LPS-stimulated macrophages by blocking NF-kappaB pathway, *KOREAN J. PHYSIOL. PHARMACOL.* 19 (2015) 211–218.
- [40] J.M. Jaynes, R. Sable, M. Ronzetti, W. Bautista, Z. Knotts, A. Abisoye-Ogunniyan, D. Li, R. Calvo, M. Dashnyam, A. Singh, T. Guerin, J. White, S. Ravichandran, P. Kumar, K. Talsania, V. Chen, A. Ghebremedhin, B. Karanam, A. Bin Salam, R. Amin, T. Odzorig, T. Aiken, V. Nguyen, Y. Bian, J.C. Zarif, A.E. de Groot, M. Mehta, L. Fan, X. Hu, A. Simeonov, N. Pate, M. Abu-Asab, M. Ferrer, N. Southall, C.Y. Ock, Y. Zhao, H. Lopez, S. Kozlov, N. de Val, C.C. Yates, B. Baljinnnyam, J. Marugan, U. Rudloff, Mannose receptor (CD206) activation in tumor-associated macrophages enhances adaptive and innate antitumor immune responses, *Sci. Transl. Med.* 12 (2020), eaax6337.
- [41] J. Shi, Y. Zhao, Y. Wang, W. Gao, J. Ding, P. Li, L. Hu, F. Shao, Inflammatory caspases are innate immune receptors for intracellular LPS, *Nature* 514 (2014) 187–192.
- [42] Z. Zhang, Y. Zhang, S. Xia, Q. Kong, S. Li, X. Liu, C. Junqueira, K.F. Meza-Sosa, T.M. Y. Mok, J. Ansara, S. Sengupta, Y. Yao, H. Wu, J. Lieberman, Gasdermin E suppresses tumour growth by activating anti-tumour immunity, *Nature* 579 (2020) 415–420.